ELSEVIER

Surface and Coatings Technology 163–164 (2003) 435–443

SURFACE & COATINGS TECHNOLOGY

www.elsevier.com/locate/surfcoat

Nano-rheological properties of polymeric third bodies generated within fretting contacts

A. Chateauminois[a,*], B.J. Briscoe[b]

[a]*Laboratoire de Physico-Chimie Structurale et Macromoléculaire, UMR CNRS 7615, Ecole Supérieure de Physique et Chimie Industrielles (ESPCI), 10 rue Vauquelin, 75005 Paris, France*

[b]*Department of Chemical Engineering, Imperial College of Science, Technology and Medicine, Prince Consort Road, London SW7 2 BY, UK*

Abstract

The accumulation and compaction of polymer wear particles into coherent third body compacts has been investigated in a contact between steel and poly(methylmethacrylate) under small amplitude cyclic micro-motions, i.e. fretting. Under such contact conditions, the preferential accumulation of the PMMA wear particles at the centre of the contact was found to result in the formation of a distinct third body agglomerate. Hardness and modulus measurements carried out at the nanoscale revealed that the polymer wear particles within this third body formation were progressively compacted to form an agglomerate, for which the mechanical properties were ultimately close to those of the initial PMMA substrate. The efficiency of the third body compaction process was interpreted by considering the evolving load-carrying capacity of the contact, which was characterised by progressive redistribution of the contact pressure within the third body layer. In addition, an assessment of the dissipation of frictional energy within the worn contact area demonstrated that particle compaction was enhanced by the highly energy-intensive nature of the fretting process.

Keywords: Poly(methylmethacrylate) (PMMA); Third body; Fretting wear; Nanoindentation; Hardness; Debris compaction

1. Introduction

Various investigations of interfacial tribology [1,2] have established that the wear resistance of tribological systems is largely governed by the debris that are usually trapped within the contact for varying periods of time, where the debris particles are subjected to a variety of processes, such as comminution, chemical reactions, aggregation and compaction, and ultimately form what is often called a third body. Most of these third bodies provide some form of protection against the wear of the 'first bodies', i.e. the primary contacting surfaces. Amongst various possible mechanisms, the difference in the velocities of the contacting surfaces can, for example, be accommodated through the shearing or rolling of the third body layer, which reduces the degradation of the first bodies [2,3]. The effectiveness of such a protection mechanism, basically a lubrication process, mainly relies upon the rheological properties of the third body, which governs its ability to flow within the interface zone and to be eventually displaced from the contact. Unfortunately, the very small length scales associated with solid third-body formations (typically of the order of a few μm), as well as their heterogeneous nature, have precluded any detailed access to quantitative and reliable data on third body rheology. This is probably one of the main reasons why interfacial tribology models do not include third body behaviour.

The recent development of depth-sensing indentation techniques at the nanometer scale, commonly known as nanoindentation, has, however, offered new opportunities in the characterisation of third bodies. Nanoindentation allows highly localised hardness and modulus measurements to be performed on very small material volumes and is particularly suitable for the study of third bodies. Recently, investigations by Randall and coworkers [4,5] and Friedrich et al. [6] have demonstrated that nanoindentation is a viable technique for measuring the hardness of thin transfer films and correlating that response with wear processes. The motivation for the

*Corresponding author. Tel: +33-1-40-79-47-87; fax: +33-1-40-79-46-86.

E-mail address: antoine.chateauminois@espci.fr (A. Chateauminois).

0257-8972/03/$ - see front matter © 2002 Elsevier Science B.V. All rights reserved.
PII: S0257-8972(02)00640-0

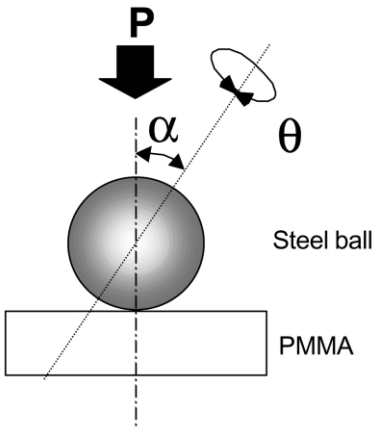

Fig. 1. Schematic description of the contact loading configuration.

present study was to investigate the potential of nanoindentation techniques in the context of the mechanical characterisation of specific polymer third-body formations previously observed under small-amplitude cyclic sliding micro-motions, i.e. fretting, within contacts between poly(methylmethacrylate) (PMMA) and steel [7,8]. Under such contact conditions, the rheological behaviour of the wear particles appeared as a particularly relevant factor in defining the wear behaviour of the polymeric material. In order to assess the level of compaction of the polymer wear debris within the third body, the distribution of hardness and modulus properties has been investigated as a function of the number of cycles. The interrelationship between the rheological properties of the third body agglomerate and the mechanical processes occurring within the degraded contact area are also discussed.

2. Experimental details

2.1. Materials and fretting experiments

The polymeric third body under investigation was generated within fretting contact between a commercial grade of cast poly(methylmethacrylate) (Perspex®, ICI Acrylics, UK) and an AISI 52100 standard bearing ball (radius 11.5 mm). The experiments consisted of applying oscillating, rotational micro-motions to the steel ball contacting the flat PMMA specimen under a constant applied normal load (20 N). The fretting device, which is fully described elsewhere [8], was designed in order to vary the angle, α, between the axis of rotation of the steel ball and the normal to the surface of the PMMA specimen (Fig. 1). In such a manner, it was possible to combine, to various extents, rotational and linear sliding motions within the contact. Within the context of this study, investigations were focused on the well-defined third body formation (see below) induced under predominantly linear sliding motion, i.e. $\alpha = 90°$. Under the specified loading conditions, the peak-to-peak amplitude of the twist angle imposed on the steel ball was set to $\theta^* = 1°$. The frequency of the fretting oscillations was 1 Hz. A separate mechanical investigation of these contact conditions [9] indicated that the resulting amplitude of actual sliding at the contact interface was approximately 120 μm, i.e. much less than the diameter of the initial Hertzian contact area (720 μm). SEM observations of the steel counterface did not reveal any notable damage after 10^4 fretting cycles.

2.2. Nanoindentation experiments

Nanoindentation experiments were carried out using commercially available apparatus (Nanoindenter II, MTS, USA) operated under load-control conditions. In the case of materials exhibiting time-dependent mechanical behaviour, it has been shown to be of primary importance to perform the indentation tests at a constant nominal strain rate [10], the latter being defined as the instantaneous descent rate of the indenter (dh/dt) divided by the displacement at that instant in time. The requirement for a constant strain rate can be fulfilled during a load-controlled indentation procedure by maintaining constant the ratio of the loading rate, $L^o = dL/dt$, to the applied load, L. In the present investigation, a constant L^o/L ratio equal to 0.05 s^{-1} was achieved by selection of an exponential loading rate. The indenter was loaded until a specified value of the indentation load, which was held constant for 100 s. At the end of this creep segment, the specimens were unloaded at 100 nm s^{-1}. These procedures have been described elsewhere in the context of glassy polymers, including PMMA [11,12]. As is described in these references, the constant load segment has the advantage of eliminating viscoelastic creep effects, which may dramatically affect measurement of the contact compliance at the onset of unloading. The indentation system also has the ability to measure continuously the dynamic contact stiffness during indentation. This is accomplished by superimposing a small-amplitude oscillation in the driving force and measuring the displacement response (approx. 1 nm) at a chosen frequency, here 40 Hz. This continuous stiffness monitoring allowed measurement of the material hardness and Young's modulus during the entire loading segment.

3. Results

3.1. Generation of PMMA third-body formations under fretting conditions

The fretting displacement amplitude selected was of the order of 100 μm, while the characteristic length of the contact was of the order of several 100 μm. Clearly, any debris detached from the contacting surfaces will

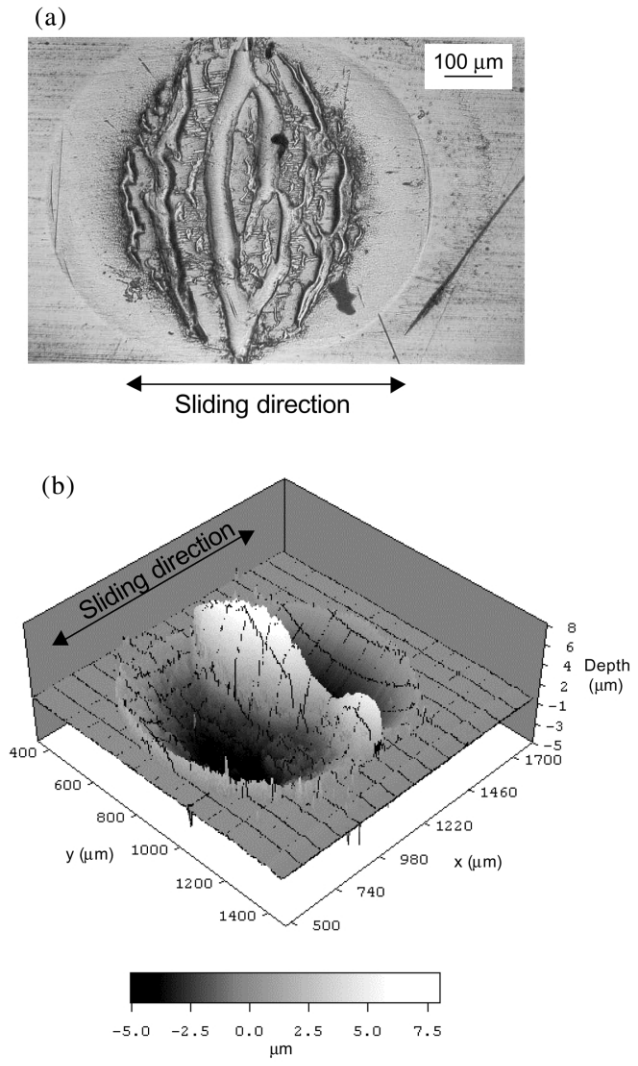

Fig. 2. Formation of the PMMA third-body agglomerate under linear sliding-fretting contact conditions (actual sliding amplitude at the contact interface: 120 μm). (a) Optical micrograph of the wear scar after 10^3 fretting cycles. (b) Topography of the wear scar after 10^4 fretting cycles.

initially be trapped within the contact. The initial debris entrapping process is thus essentially a geometrical effect. The subsequent retention of debris within the contact involves, however, a much more complex phenomenon, primarily depending on third body rheology and the details of contact zone kinematics. This latter aspect was reported in previous studies [7], which indicated that very low wear volumes could be achieved under linear sliding conditions as compared to torsional contact conditions. This enhanced wear resistance was associated with the progressive formation of a stable polymer third-body medium, which was able to accommodate, by a shearing process, a substantial fraction of the imposed relative displacement between the primary contacting surfaces. Basically, as shown in Fig. 2a, these third body structures consisted of thin ripples oriented perpendicular to the sliding direction. As the number of fretting cycles was increased, the formation of a single ripple was eventually observed (Fig. 2b). In situ visualisation of the contact during fretting tests did not show any evidence of transfer of the PMMA wear debris to the steel counterface. Sliding micro-motions therefore occurred at the interface between the third body compact and the steel ball. Topographical analysis of the wear scars revealed that the third body corrugations obtained after 10^4 fretting cycles consisted of distinct, flattened ribbons, typically 10 μm thick and 100 μm in width, which were partially indented into the PMMA substrate. An analysis detailed elsewhere [8] indicated that the heterogeneous nature of particle detachment processes in relation to the evolving contact-zone kinematics within the degraded contact area could account for these observations. Another important aspect is certainly the rheological behaviour of the polymer particles agglomerate, which governs its ability to flow within the contact under the action of the imposed shear stresses. This aspect was further investigated by performing nanoindentation experiments within selected areas of the PMMA third-body compact.

3.2. Third body nano-mechanical properties

3.2.1. Analysis of the third body indentation behaviour

Using the positioning location facility of the nanoindenter specimen stage, it was possible to select various indentation areas within the third body agglomerate with a spatial resolution of a few μm. The maximum load selected (i.e. 6 mN) ensured that the indentation depth, h_t, did not exceed 2.0 μm, i.e. less than one-fifth of the average thickness of the third body formation. A first examination of the indentation results after 5×10^3 fretting cycles revealed that, depending upon the location of the indent within the third body, two kinds of response, hereafter denoted as type I and II, were distinguished (Fig. 3). For type I indentation responses, the loading and unloading curves were nearly identical to those of the virgin PMMA. The only difference compared to PMMA consisted of a slightly higher creep-indentation rate of the third body agglomerate during the constant-load segment (210 ± 50 vs. 130 ± 5 nm for the virgin PMMA). On the other hand, type II behaviour was characterised by a very different indentation response during both the loading and unloading steps. During loading, a significant departure was observed from the classical power law response ($L\propto h_t^2$) which is characteristic of homogeneous materials. In addition, much higher total indentation depths were achieved, which could be attributed to reduced cohesiveness of the wear debris agglomerate. In Fig. 3, it can also be noted that the extent of elastic recovery during unloading appears more limited than for the virgin PMMA, as indicated by the reduced curvature of the unloading

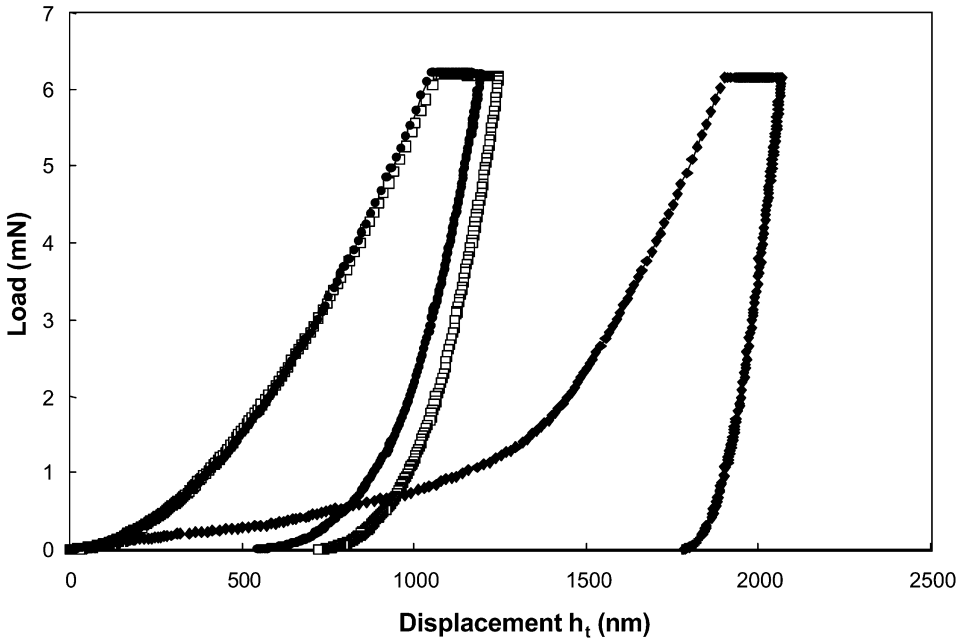

Fig. 3. Typical indentation response of the PMMA substrate and the third body generated after 5×10^3 fretting cycles. (●) virgin PMMA; (□) third body exhibiting type I behaviour; and (◆) third body exhibiting type II behaviour.

curves. In the context of homogeneous materials, this latter feature is often associated with predominantly rigid–plastic behaviour.

Further insight into the mechanical response of the third body agglomerate can be provided by examination of the dynamic contact stiffness, S. In Fig. 4, S has been represented as a function of the computed 'plastic depth', h'_r, which was defined as follows [13]:

$$h'_r = h_t - L/(\gamma S) \quad (1)$$

where h_t is the measured indentation depth, L is the load and γ is a correction factor that takes into account the dynamic effects associated with measurement of the contact stiffness at 40 Hz. According to Hochstetter et al. [11], the value of γ (0.85) was determined from the ratio of the quasi-static contact stiffness determined at the onset of unloading to the dynamic stiffness measured at the same indentation depth.

For a material having a constant Young's modulus through the thickness, such as fused silica, a linear relationship is usually observed between the contact stiffness and h'_r. This linear behaviour can be justified by Sneddon's analysis [14], which states that there is a linear relationship between the contact stiffness and the square root of the projected contact area, A:

$$S = 2E_r\sqrt{A/\pi} \quad (2)$$

where E_r is the reduced modulus. By virtue of the shape of the Berkovich indenter (equivalent to a conical indentor having a 70.3° tip half-angle), the contact depth is proportional to the square root of the contact area. It therefore transpires from Eq. (2) that the observed linearity of the stiffness vs. h'_r relationship can be considered as an indication of the constancy of the Young's modulus through the thickness.

Such a linear behaviour was indeed observed for PMMA and for third body indents exhibiting type I behaviour (Fig. 4). Interestingly, the nearly identical slopes indicate that the reduced modulus of the type I third body is the same as that of the virgin PMMA surface. Both stiffness and load/displacement data, therefore, consistently provide the conclusion that, at least in some parts of the wear scars corrugations, the mechanical response of the third body agglomerate is very similar to that of the homogeneous substrate from which it originates.

In contrast, type II behaviour was characterised by a strongly non-linear response. The heterogeneous distribution of the mechanical properties within some less compacted wear-debris regions could account for these observations. There was, however, no evidence of the small stochastic drops (pop-in) that may sometimes occur in less coherent agglomerate systems due to localised failure events between particles [15]. Two other aspects need consideration regarding the complex type II response. The first is related to the increased roughness of the third body corrugations, as compared to the initially relatively smooth surface of the cast PMMA. As shown in Fig. 5, typical asperity heights within the central flattened part of the third body roll can be of the order of a few 100 nm, which is not negligible with respect to the indentation depths. Although a compre-

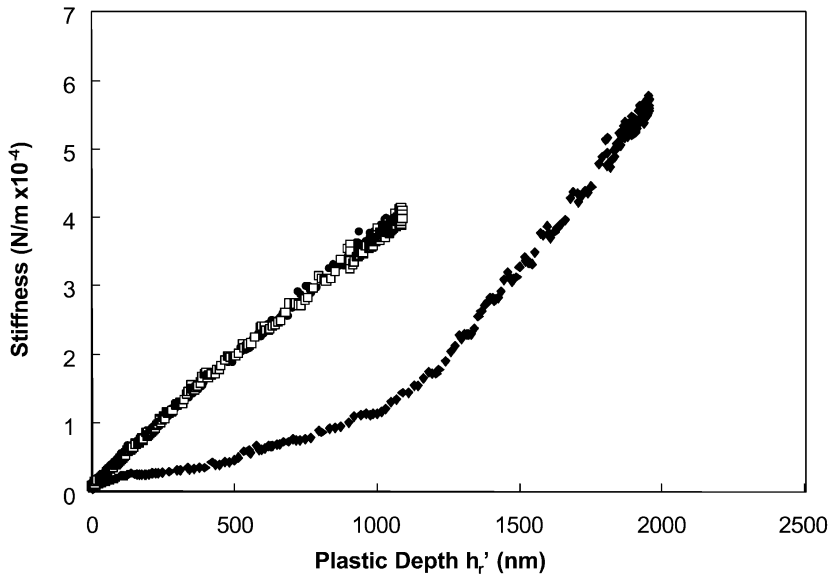

Fig. 4. Dynamic contact stiffness as a function of the plastic depth: (●) virgin PMMA; (□) third body exhibiting type I behaviour; and (♦) third body exhibiting type II behaviour.

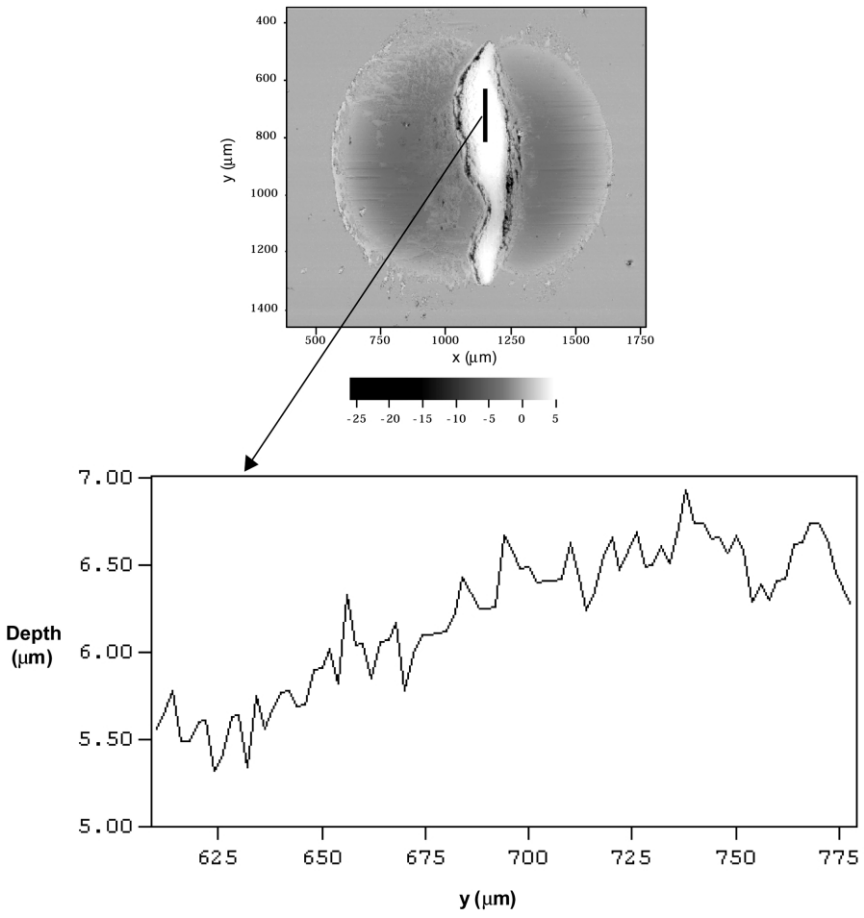

Fig. 5. Roughness profile within the third body agglomerate (from laser profilometry measurements, 5×10^3 fretting cycles).

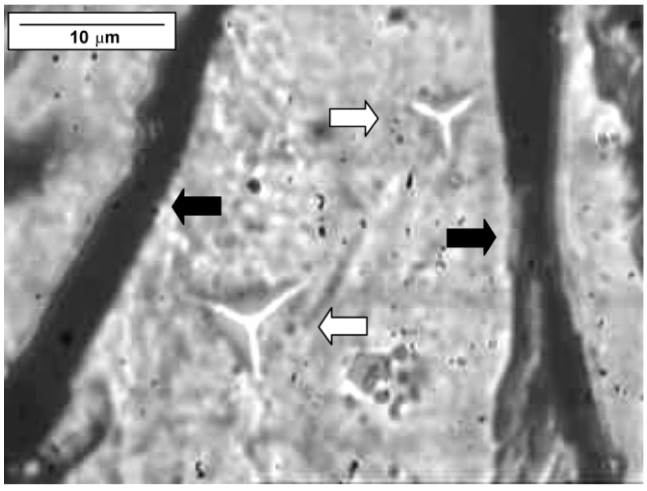

Fig. 6. Optical micrographs showing cracks within the third body close to indents (indent locations indicated by white arrows; cracks indicated by black arrows).

hensive treatment of roughness effects during indentation is beyond a simple analysis, the complex interactions between the indenter tip and the surface asperities could induce some perturbations in the initial indentation response of the third body. Another important aspect is the existence of surface discontinuities, such as cracks, which were induced by shearing of the third body layer during the sliding process. During the nanoindentation experiments, it proved to be difficult to ensure that some of the selected indent locations were not close to these cracks (Fig. 6). As a result, some of the type II indentation responses measured could possibly involve some slip between the faces of these internal cracks during indentation loading and unloading.

3.2.2. Assessment of the distribution of hardness and modulus properties within the third body

Assuming a constant reduced modulus, the material hardness, H, can be computed as a function of depth from the raw displacement/load/stiffness data following the method of Bec et al. [16]. The contact depth, h_c, was calculated from the measured value of the plastic depth, h'_r, using the following relationship:

$$h_c = \alpha(h'_r + h_1) \quad (3)$$

where α is an empirical constant close to 1.2 and h_1 is an apparent tip defect close to 30 nm, which was estimated by extrapolating to zero stiffness the $S = f(h'_r)$ linear relationship [11]. From the contact depth, the projected contact area, A, was subsequently calculated using the following expression:

$$A = \beta h_c^2 = \beta\{\alpha(h'_r + h_1)\}^2 \quad (4)$$

where β is a shape factor equal to 24.56 for a Berkovich indenter. Finally, the hardness is simply given by $H = L/A$. From the linearity of the stiffness vs. plastic depth relationship, it was concluded that virgin PMMA and type I third-body regions exhibit a constant reduced modulus, which is consistent with the basic hypothesis of the above analysis. In this case, constant and similar hardness values were obtained over the indentation depths sensed (Fig. 7). For the type II indentation response, only 'apparent' hardness values can be calculated, as the constant modulus assumption is obviously no longer valid in this case. Although these hardness

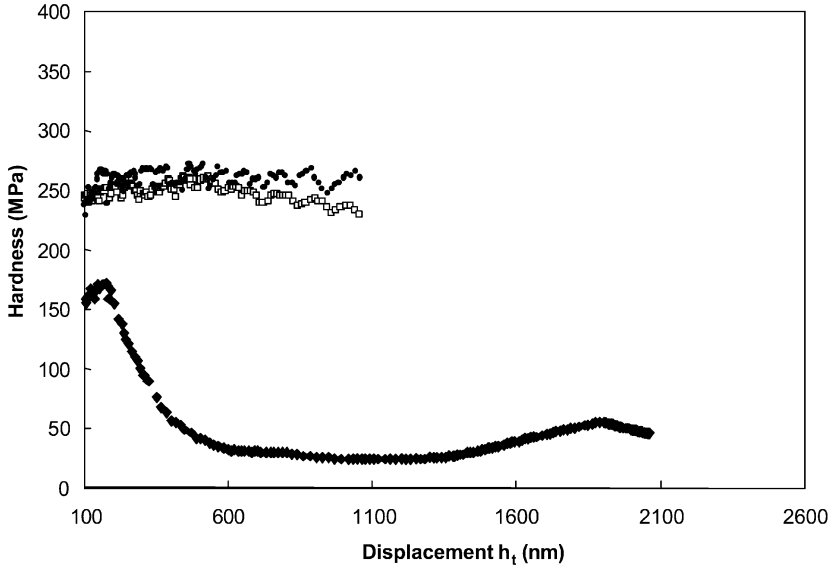

Fig. 7. Hardness profiles for: (●) virgin PMMA; (□) third body exhibiting type I behaviour; and (♦) third body exhibiting type II behaviour (5×10^3 fretting cycles).

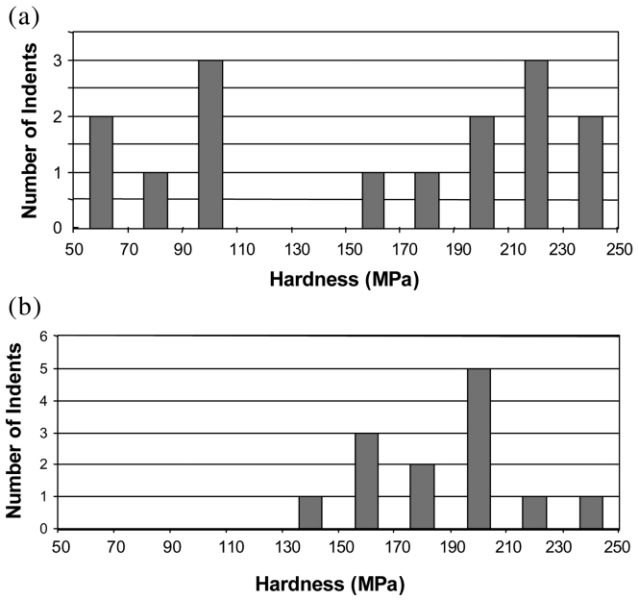

Fig. 8. Histograms showing the distribution of hardness after (a) 5×10^3 and (b) 10^4 fretting cycles.

data no longer correspond to well-defined material properties, they were used in the context of this study to quantify the deviation of the third body behaviour from a reference corresponding to the PMMA substrate. Fig. 7 shows a typical example of the apparent hardness profiles generated with data obtained from a type II indentation response. In addition to low calculated hardness values, the profile shows strongly depth-dependent behaviour, which is consistent with the conclusions provided by the contact stiffness measurements.

The histograms reported in Fig. 8 give an indication of the distribution of the hardness properties within the third body corrugations as a function of the number of fretting cycles. For 5×10^3 cycles, two distinct populations can be clearly distinguished. When the number of cycles is increased (up to 10^4), the low-hardness indents population tends to disappear and the third body properties become, on average, more homogeneous and closer to those of the original PMMA substrate. As strong modifications in the topography or density, or shear-induced cracks are not likely to occur at the same time within the third body corrugations, it can be stated that the changes observed in the apparent hardness indeed reflect progressive compaction of the wear debris within an increasingly coherent third-body layer, for which the mechanical properties become ultimately close to those of the PMMA.

4. Discussion

Although analysis of the nanoindentation experiments carried out within wear debris formations is complicated by some additional difficulties arising from surface roughness effects and by the existence of macroscopic defects, such as cracks, the present investigation clearly demonstrates that, under specific contact-zone kinematic conditions, the fretting wear of PMMA can result in the progressive formation of a highly coherent and homogeneous third body layer. One of the main consequences of this progressive increase in the third-body mechanical behaviour is probably to limit the rate of third-body flow out of the contact. Such an assumption is consistent with the reduced wear volumes measured when a third body agglomerate was trapped at the contact interface [7]. A connection can thus be established between particle migration and compaction within coherent third-body agglomerates and the ultimate wear degradation of the polymer.

Basic understanding of the physical and mechanical processes involved in the formation of such coherent third-body layers remains, however, obscure for several reasons. The main one is probably the lack of information regarding the initial size of debris particles and their formation mode. Even with the resources of in situ optical microscopy, it proved to be very difficult to capture the initial stages of debris formation within the macroscopic fretting contacts under consideration. Once formed, debris particles can change in size and shape due to the crushing action of the rubbing surfaces, and the wear debris observed within the resolution of optical microscopy does not necessarily reflect the initial morphology. Particle size is probably a very important issue during third-body particle agglomeration and compaction, especially if initial wear debris detachment processes involve the formation of particles in the sub-micrometer range. Recent developments in the rapidly evolving area of the study of glass transition of polymer films have demonstrated that confinement effects on polymer dynamics can result in significant reduction of the glass transition temperature of thin ($<$ 500 Å) amorphous polymer films, including PMMA (see [17] for a review). Such effects in the context of the compaction of very fine wear debris could result in an enhanced contribution from adhesive processes during the initial stages of debris compaction. It must, however, be noted that the hydrostatic pressure component associated with normal contact loading results in an opposite effect, namely an increase in the glass transition. Previously reported results concerning the friction of thin PMMA films [18] indicate that this effect should be limited for the nominal contact pressure (approx. 50 MPa) encountered in the fretting contacts under investigation.

As the size of third body debris increased well into the micrometer range, the contribution of additional mechanical processes to debris compaction can be envisaged. The first is related to the evolving load-carrying capacity of the contact. By virtue of wear debris accumulation within restricted regions of the worn contact

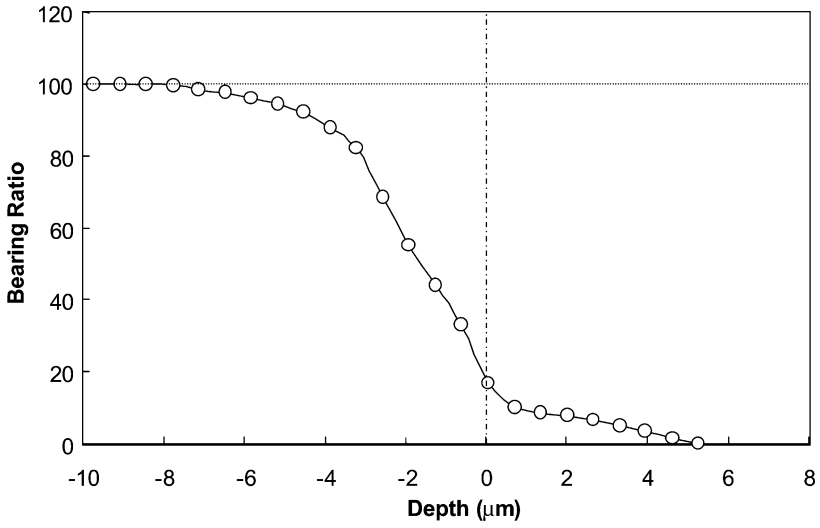

Fig. 9. Bearing ratio curve of the PMMA wear scar after 10^4 fretting cycles (the initial unworn surface of the PMMA substrate has been taken as a reference for the depth measurements).

area, the normal pressure distribution can be altered in the same way, for instance, that an oil film modifies the pressure distribution obtained in a dry contact. This hypothesis of an evolving contact load-carrying capacity is further supported by previously reported in situ observation of the contact, which indicated that the primary rubbing surfaces were progressively separated by the third body layer [8]. A simple way to quantify the changes in the contact load-carrying capacity is to analyse the wear scar topography by means of the so-called 'Abbot's curves' or bearing ratio curves. Although this simple approach does not take into account the deformation processes within the third body and the surrounding PMMA substrate, it provides an approximate estimate of the local contact pressure that may be achieved within the agglomerate. For example, a typical value of the bearing ratio close to 20% (Fig. 9) yields a contact pressure of approximately 250 MPa within the third body corrugation. This value cannot be directly compared to the indentation hardness (the high constraint factor of the third body layer within the contact can increase the flow stress by an unknown factor, which can typically be of the order of two or three), but it clearly demonstrates that, as wear proceeds, the compaction of wear particles within a coherent third body can be enhanced by the substantial increase in local contact pressure.

In addition to the effects of normal pressure, the contribution of shearing forces to the compaction of the third body agglomerate also needs to be considered. An obvious consequence of the increased contact pressure is to enhance the shear stresses transmitted to the third body layer, which can eventually largely exceed the yield strength of the PMMA. In addition to the stress-based considerations, it is also interesting to try to evaluate the amount of frictional energy available for compaction processes within the third body. As a first approach, an upper bound can be obtained by assuming that all the frictional energy is dissipated within the third body compact. The associated dissipated power, W_f, can be estimated from the following expression:

$$W_f = 2\mu PR\Theta^* \nu \tag{5}$$

where μ is the coefficient of friction, P is the normal load, R is the radius of the steel ball, Θ^* is the magnitude of the applied angle of twist and ν is the frequency. From surface strain measurements reported elsewhere [9], the coefficient of friction within the contact under investigation was found to be close to 0.75. At 1 Hz, the frictional energy dissipated per fretting cycle is thus approximately 6 mW. From topographical measurements within the wear scar before and after the wear particles were removed by ultrasonic cleaning, the average volume of the third body compact was estimated to be close to 7×10^3 μm^3 after 5×10^5 fretting cycles [7]. Using this value, the maximum frictional energy dissipated per unit of third body volume and per unit time is approximately 10^{-5} $mW/\mu m^3$. This value can interestingly be compared with the power dissipated during a nanoindentation test, which involves a substantial level of plastic deformation within the polymer. The deformation energy per displaced volume and per unit time, W_i, can be estimated from the following expression:

$$W_i = \frac{1}{V_p}\frac{1}{t_{loading}+t_{unloading}} \times\left(\int_{loading} L\,dh - \int_{unloading} L\,dh\right) \tag{6}$$

where V_p is the residual material volume displaced at the end of unloading, and $t_{loading}$ and $t_{unloading}$ are the loading and unloading time, respectively. From geometrical considerations, V_p can be defined as follows for a pyramidal indenter:

$$V_p = Ah_{res}/3 \quad (7)$$

where h_{res} is the residual indentation depth. According to Eqs. (6) and (7), analysis of a type I indentation test within the third body gives a dissipated power of approximately 10^{-9} mW/μm^3, i.e. several orders of magnitude less than for the fretting process. Although the estimate of W_f is certainly grossly overestimated because the dissipation of a part of the frictional energy as heat within the steel sphere has not been taken into account, this comparison emphasises the highly energy-intensive nature of the fretting process. Accordingly, the possibility of some thermally enhanced consolidation cannot be discarded. Although a simple thermal analysis demonstrated that the steady-state mean temperature increase within the initial, unworn, Hertzian contact area should not exceed 10 K [7], a much more substantial temperature increase could be locally achieved in the third body compact, where the redistribution of the contact load-carrying capacity induces a localisation of the frictional energy dissipation.

5. Conclusion

Sliding micro-motions in a fretting contact between steel and PMMA have been found to result in the formation of distinct polymer particle agglomerates, for which the mechanical properties in terms of hardness and modulus became close to these of the initial PMMA substrate as wear proceeds. The complex nanoindentation response of the third body formations demonstrates, however, the need for improved data processing techniques to use within the context of the nanoindentation of such heterogeneous media. This latter point is probably one of the prerequisites for the incorporation of third body mechanical behaviour within wear models.

Although understanding of the physico-mechanical mechanisms involved in polymer particle compaction at the micrometer scale needs further investigation, this study clearly demonstrates the influence of mechanical factors, such as the evolving load-carrying capacity of the contact and the highly energy-intensive nature of the fretting process, which involves a lot of redundant work within the constrained third body layers.

References

[1] M. Godet, Wear 100 (1984) 437.
[2] Y. Berthier, M. Godet, M. Brendle, Tribol. Trans. 32 (4) (1989) 490.
[3] S.M. Aharoni, Wear 25 (1973) 309.
[4] N.X. Randall, J.L. Bozet, Wear 212 (1997) 18.
[5] N.X. Randall, A. Harris, Wear 245 (2000) 196.
[6] K. Friedrich, J. Flock, K. Varadi, Z. Neder, Wear 251 (2001) 1202.
[7] B.J. Briscoe, A. Chateauminois, D. Parsonage, T.C. Lindley, Wear 240 (2000) 27.
[8] B.J. Briscoe, A. Chateauminois, T.C. Lindley, D. Parsonage, Tribol. Int. 31 (11) (1998) 701.
[9] B.J. Briscoe, A. Chateauminois, Tribol. Int. 35 (2002) 245.
[10] B.N. Lucas, W.C. Oliver, G.M. Pharr, J.L. Loubet, Time-dependent deformation during indentation testing, Material Research Society Symposium Proceedings, 1996, p. 233.
[11] G. Hochstetter, A. Jimenez, L. Loubet, J. Macromol. Sci. Phys. B 38 (5–6) (1999) 681.
[12] B.J. Briscoe, L. Fiori, E. Pelillo, J. Phys. D: Appl. Phys. 31 (1998) 2395.
[13] J.L. Loubet, J.M. Georges, G. Meille, Vickers indentation curves of elastoplastic materials, in: B.R. Lawn (Ed.), Microindentation Techniques in Materials Science and Engineering, ASTM STP 889, Philadelphia, American Society for Testing and Materials, 1986, p. 72.
[14] I.N. Sneddon, Int. J. Eng. Sci. 3 (1965) 47.
[15] M.J. Adams, A. Akram, B.J. Briscoe, C.J. Lawrence, D. Parsonage, J. Mater. Res. 14 (6) (1999) 2344.
[16] S. Bec, A. Tonck, J.M. Georges, E. Georges, J.L. Loubet, Philos. Mag. 74 (5) (1996) 1061.
[17] J.A. Forrest, K. Dalkoni-Veress, Adv. Colloid Interface Sci. 94 (2001) 167.
[18] B.J. Briscoe, A.C. Smith, The shear properties of thin organic films, Reviews on the Deformation Behaviour of Materials III, 1980, p. 151.